



# Symmetry-breaking analysis for the general Helmholtz–Duffing oscillator

Hongjun Cao <sup>a,b,\*</sup>, Jesús M. Seoane <sup>b</sup>, Miguel A.F. Sanjuán <sup>b</sup>

<sup>a</sup> *Department of Mathematics, School of Science, Beijing Jiaotong University, Beijing 100044, PR China*

<sup>b</sup> *Nonlinear Dynamics and Chaos Group, Departamento de Ciencias de la Naturaleza y Física Aplicada, Universidad Rey Juan Carlos, Tulipán s/n, 28933 Móstoles, Madrid, Spain*

Accepted 6 April 2006

## Abstract

The symmetry breaking phenomenon for a general Helmholtz–Duffing oscillator as a function of a symmetric parameter in the nonlinear force is investigated. Different values of this parameter convert the general oscillator into either the Helmholtz or the Duffing oscillator. Due to the variation of the symmetric parameter, the phase space patterns of the unperturbed Helmholtz–Duffing oscillator will cause a huge difference between the left-hand homoclinic orbit and the right-hand one. In particular, the area of the left-hand homoclinic orbits is a strictly monotonously decreasing function, while the area of the right-hand homoclinic orbit varies only in a very small range. There exist distinct local supercritical and subcritical saddle-node bifurcations at two different centers. The left-hand and the right-hand existing regions of the harmonic solutions of the Helmholtz–Duffing oscillator created by the left-hand and the right-hand saddle-node bifurcation curves will lead to different transition in the amplitude–frequency plane. There exists also a critical frequency which has the effect that the left-hand homoclinic bifurcation value is equal to the right-hand homoclinic bifurcation value. And, if the amplitude coefficient of the Helmholtz–Duffing oscillator is used as the control parameter, and it is larger than the same left-hand and right-hand homoclinic bifurcation, then the global stability of the system will be destroyed at a lowest cost. Besides this critical frequency, the left-hand and the right-hand homoclinic bifurcations are not only unequal, but also their effects for the system's stability are different. Among them, the effect resulting from the small homoclinic bifurcation for the system's stability is local and negligible, while the effect from the large homoclinic bifurcation is global but this is accomplished at a quite larger cost.

© 2006 Elsevier Ltd. All rights reserved.

## 1. Introduction

There are many phenomena and real applications related to the symmetry breaking phenomenon [1–5] in the fields of scientific research and engineering. For instance, a ship dynamics will be affected under the action of waves and the unbalance cargo [1]; in the electric power system, the users of a local and global electrical grid are always unbalanced

\* Corresponding author. Address: Department of Mathematics, School of Science, Beijing Jiaotong University, Beijing 100044, PR China. Tel.: +86 10 51682 056; fax: +86 10 51688 433.

E-mail addresses: [hjcao@center.njtu.edu.cn](mailto:hjcao@center.njtu.edu.cn), [hongjun.cao@urjc.es](mailto:hongjun.cao@urjc.es) (H. Cao).

during different periods of time [6–9]. In addition, the simplest physical platform concerning the symmetry breaking can be designed as follows [10]: a small ball (or a particle) is placed in an asymmetric double-well potential with the base vibrating harmonically. The asymmetric two-well potential has two equilibria when the base does not vibrate. When the base vibrates periodically with a large enough amplitude, the small ball will jump from one well to the other in an apparently random manner. Due to the asymmetry of the double-well potential, the system may exhibit much more complicated dynamical behaviors, for example, at least two types of motion can be observed (they can be either regular or chaotic): (a) the oscillation confined to one of the potential wells; and (b) the rotation or cross-well motion, when the small ball escapes out of the potential well overcoming the potential barrier.

Over the past decades, concerning the study about the symmetry breaking phenomenon of the nonlinear oscillator, the following works attract our attention. In 1994, Yagasaki [11] considered the following pendulum oscillator:

$$\begin{aligned}\dot{x} &= y, \\ \dot{y} &= -\sin x - \alpha x + \beta - \delta y + \gamma \cos(\omega t).\end{aligned}\quad (1)$$

Eq. (1) includes a parameter  $\beta \neq 0$ , so that the unperturbed system of Eq. (1) possesses a pair of asymmetric homoclinic orbits with respect to fixed parameters  $\alpha$  and  $\beta$ . By using the Melnikov method, Yagasaki obtained two different homoclinic bifurcations.

Litvak-Hinenzon and Rom-Kedar [12] considered another oscillator

$$\begin{aligned}\dot{x} &= y, \\ \dot{y} &= x - x^3 - \delta y + (x - \beta x^2)\gamma \cos(\omega t),\end{aligned}\quad (2)$$

in which there is a parameter  $\beta$  associated to the asymmetric periodic perturbation. Their investigation shows that the bifurcations and strange attractors of Eq. (2) will produce the substantial changes when the parameter  $\beta$  varies.

Recently, Lenci and Rega [13,14] considered the Helmholtz–Duffing oscillator as follows:

$$\begin{aligned}\dot{x} &= y, \\ \dot{y} &= \sigma x + \frac{3}{2}(\sigma - 1)x^2 - 2x^3 - \delta y + \gamma \cos(\omega t).\end{aligned}\quad (3)$$

Eq. (3) is also an asymmetric oscillator when the asymmetric parameter  $\sigma \neq 1$ . In [13,14], the main goal of Lenci and Rega is to control the asymmetric left-hand or/and right-hand homoclinic bifurcations using the optimal control technique.

In addition, Almendral et al. [15] and Almendral and Sanjuán [16] considered the simplest asymmetric nonlinear oscillator which is the nonlinear Helmholtz oscillator. The main result is to obtain the corresponding symmetries and conditions for the complete integrability of the system when a linear damping is considered.

An interesting analysis of the effect of nonlinear damping on the Helmholtz oscillator was carried out in [17].

Although much more progress have been made in the study for the symmetry breaking phenomenon of the nonlinear oscillators, new problems are always appearing. We can often see the latest reports about the symmetry breaking in the scientific literature. But, few of these reports consider the deep reason leading to the symmetry breaking in nature, and most of them are limited in the reports for various exterior forms of the symmetry breaking.

Based on these reasons above, we consider the following nonlinear oscillator as an archetype in this paper

$$\ddot{x} + \delta \dot{x} - x + (1 - \sigma)x^2 + \sigma x^3 = \gamma \cos(\omega t),\quad (4)$$

or its equivalent form:

$$\begin{aligned}\dot{x} &= y, \\ \dot{y} &= x - (1 - \sigma)x^2 - \sigma x^3 - \delta y + \gamma \cos(\omega t),\end{aligned}\quad (5)$$

where  $\delta y$  stands for the damping term with the damping coefficient  $\delta$ . Let  $f(x) = \sigma x^3 + (1 - \sigma)x^2 - x$ , and  $f(x)$  denotes the nonlinear force with a symmetric parameter  $\sigma$ ;  $\gamma \cos(\omega t)$  is an external periodic forced term with the periodic  $T = 2\pi/\omega$ .

When  $\sigma = 1$ , Eq. (5) is a classical Duffing oscillator, while Eq. (5) becomes a Helmholtz oscillator with a single-well potential when  $\sigma = 0$ .

As a general model, Eq. (5) is of very obvious physical meaning appearing in different disciplines. For example, in the study of the single model dynamics of a one dimensional structural systems with an initial curvature [18], such as shallow arches, the system dynamics can be modelled as the similar form as Eq. (5). In the study of ship roll dynamics [19], Eq. (5) may represent the model with a constant wind load or an imbalance in cargo loading. In addition, some electrical circuits can also be simulated by the similar model as Eq. (5) [6–9].

When  $\sigma \neq 1$ , Eq. (5) is not invariant under the transformation of

$$x \mapsto -x, \quad t \mapsto t + \frac{\pi}{\omega}, \quad (6)$$

thus, we call Eq. (5) an *asymmetric Helmholtz–Duffing oscillator*.

By investigating the paradigmatic Helmholtz–Duffing oscillator, the goal of this paper is to establish a function relationship between the symmetry breaking phenomenon and the symmetric parameter. In such a way, we wish to give a unified view of the symmetry breaking behaviors of several oscillators. Concerning this main idea, the following unsolvable problems will be considered: (i) for the phase space patterns of the unperturbed system of Eq. (5), what happens when the parameter  $\sigma$  varies? (ii) how to measure qualitatively and quantitatively the difference between the distinct left-hand and right-hand homoclinic bifurcations of Eq. (5)? (iii) when there exist the distinct left-hand and right-hand homoclinic bifurcations of Eq. (5), what results will happen corresponding to the symmetry breaking phenomenon? (iv) what relationship exists between the symmetry breaking phenomenon and the system's local and global instabilities?

The rest of this paper is organized as follows: Section 2 presents some properties of the unperturbed system of Eq. (5) corresponding to various parameter values of  $\sigma$ . Section 3 discusses the local bifurcations of Eq. (5) at two different centers when  $\sigma \neq 1$ . In Section 4, a detailed Melnikov analysis is given. In Section 5, a theoretical analysis is verified by numerical simulations on several concerned issues including the patterns of stable and unstable manifolds and the basins of attraction. Conclusions are given in Section 6.

## 2. Analysis of the unperturbed Helmholtz–Duffing oscillator

The unperturbed system of Eq. (5) is as follows:

$$\begin{aligned} \dot{x} &= y, \\ \dot{y} &= x - (1 - \sigma)x^2 - \sigma x^3 \end{aligned} \quad (7)$$

with the potential function

$$V(x) = -\frac{x^2}{2} + \frac{1 - \sigma}{3}x^3 + \frac{\sigma}{4}x^4. \quad (8)$$

Thus, Hamiltonian function associated to Eq. (7) is

$$H(x, y) = \frac{y^2}{2} - \frac{x^2}{2} + \frac{1 - \sigma}{3}x^3 + \frac{\sigma}{4}x^4. \quad (9)$$

For the unperturbed system, (Eq. (7)), when  $\sigma \neq 0$ , there exist three fixed points:  $(0, 0)$  is a hyperbolic saddle point,  $(x_{-1}, 0) = (-1/\sigma, 0)$  and  $(x_1, 0) = (1, 0)$  are two different centers. When  $\sigma = 0$ , there are only two fixed points for Eq. (7), where  $(0, 0)$  is still a hyperbolic saddle point, but  $(x_1, 0) = (1, 0)$  is a unique center.

Note that when  $\sigma \neq 0$ , the saddle point  $(0, 0)$  and the right-hand center  $(1, 0)$  are always fixed, but the position of the left-hand center  $(-1/\sigma, 0)$  can be changed along the  $x$ -axis back and forth by increasing or decreasing the parameter  $\sigma$ . In particular, only in the case  $\sigma = 1$ , the left-hand center is symmetric to the right-hand center.

Suppose that  $H(x, y) = 0$ , which denotes the homoclinic orbits of the unperturbed system through the saddle point  $(0, 0)$ , then we can solve the two intersection points between the homoclinic orbits and the  $x$ -axis as follows:

$$x_{l,r} = \frac{2(\sigma - 1) \mp \sqrt{2}\sqrt{2\sigma^2 + 5\sigma + 2}}{3\sigma}, \quad (10)$$

where and throughout this paper, the letters “l” and “r” stand for the left-hand side and the right-hand side, respectively.

The total energy or the Hamiltonian function value through the saddle point  $(0, 0)$  is  $H(0, 0) = 0$ . When  $H < 0$ , there exist two families of periodic orbits inside the left-hand side and the right-hand side of homoclinic orbits, respectively. They correspond to the oscillations inside the homoclinic orbits of the unperturbed system; when  $H > 0$ , there exist another family of rotations outside the homoclinic orbits of the unperturbed system. Usually, the internal oscillations are stable in the absence of damping and periodic perturbations. But, under the perturbation of damping and periodic forced terms, the internal oscillations could escape from the potential wells of the system.

In order to measure qualitatively and quantitatively the sizes of the left-hand and the right-hand potential wells when the parameter  $\sigma$  varies, the two minima of the potential function  $V(x)$  are obtained as follows:

$$V_1^{\min}(x_{-1}) = -\left(\frac{1}{6\sigma^2} + \frac{1}{12\sigma^2}\right), \quad V_r^{\min}(x_1) = -\left(\frac{1}{6} + \frac{\sigma}{12}\right). \tag{11}$$

The distance between these minima and the  $x$ -axis can be measured by the following formulae:

$$d_l = |V_1^{\min}(x_{-1})| = \frac{1}{6\sigma^2} + \frac{1}{12\sigma^2}, \quad d_r = |V_r^{\min}(x_1)| = \frac{1}{6} + \frac{\sigma}{12}. \tag{12}$$

And it is easy to get the following conclusion:

$$\begin{aligned} \lim_{\sigma \rightarrow 0^+} V_1^{\min}(x_{-1}) &= -\infty, & \lim_{\sigma \rightarrow +\infty} V_1^{\min}(x_{-1}) &= 0, \\ \lim_{\sigma \rightarrow 0^+} V_r^{\min}(x_1) &= -\frac{1}{6}, & \lim_{\sigma \rightarrow +\infty} V_r^{\min}(x_{-1}) &= -\infty. \end{aligned} \tag{13}$$

Therefore, the four cases can be divided into: (i) if  $\sigma = 0$ , then Eq. (5) corresponds to the oscillator with the single potential well; (ii) if  $0 < \sigma < 1$ , then  $d_l > d_r$ , which means that the size of the left-hand potential is larger than the right-hand one; (iii) if  $\sigma = 1$ , then  $d_l = d_r$ , which means that the size of the left-hand potential and the size of the right-hand one are the same; (iv) if  $\sigma > 1$ , then  $d_l < d_r$ , which means that the size of left-hand potential is less than the right-hand one. In addition, the larger the  $\sigma$ , then the lesser the size of the left-hand potential well. Otherwise, the lesser the  $\sigma$ , then the larger the size of the left-hand potential well. While, the right-hand case is different with our common sense. Corresponding to the four cases listed above, some representative potential functions and phase space portraits are presented in Figs. 1 and 2.

Due to the various scales used in Fig. 2, it is hard to compare their sizes of the left-hand and right-hand potential wells with respect to different parameter values  $\sigma$ . So the area curves of the left-hand side and the right-hand side of the potential wells are shown in Fig. 3, in which, the left-hand and right-hand areas  $A_l$  and  $A_r$  can be obtained by computing the following integrals:

$$A_l = 2 \int_{x_l}^0 y_0^l dx, \quad A_r = 2 \int_0^{x_r} y_0^r dx, \tag{14}$$

where  $y_0^l$  and  $y_0^r$  denote the left-hand and the right-hand homoclinic orbits of the unperturbed system, respectively.

Seen from Fig. 3, the solid line stands for the left-hand areas of the potential wells when the parameter  $\sigma$  varies in the range  $[0, 4]$ . With the increase of the parameter  $\sigma$ , the area curve of the left-hand potential well is a strictly monoto-

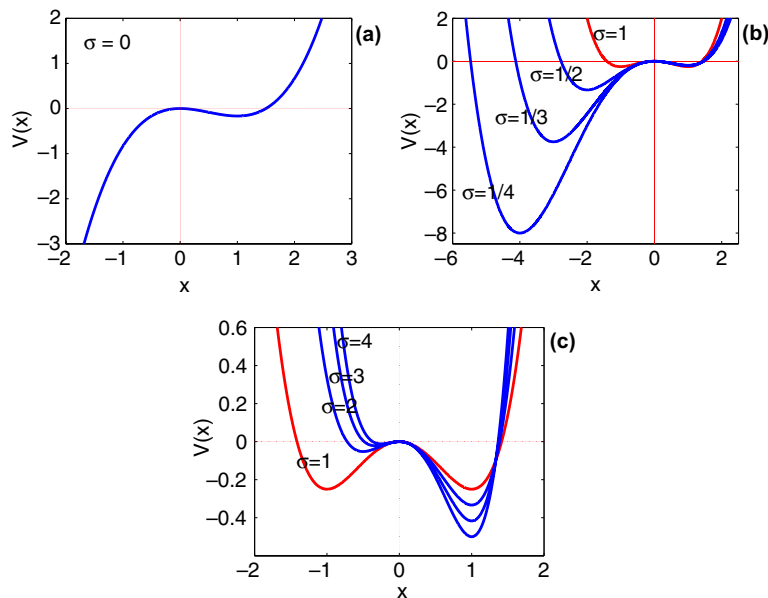


Fig. 1. Potential functions with respect to various values of parameter  $\sigma$ .

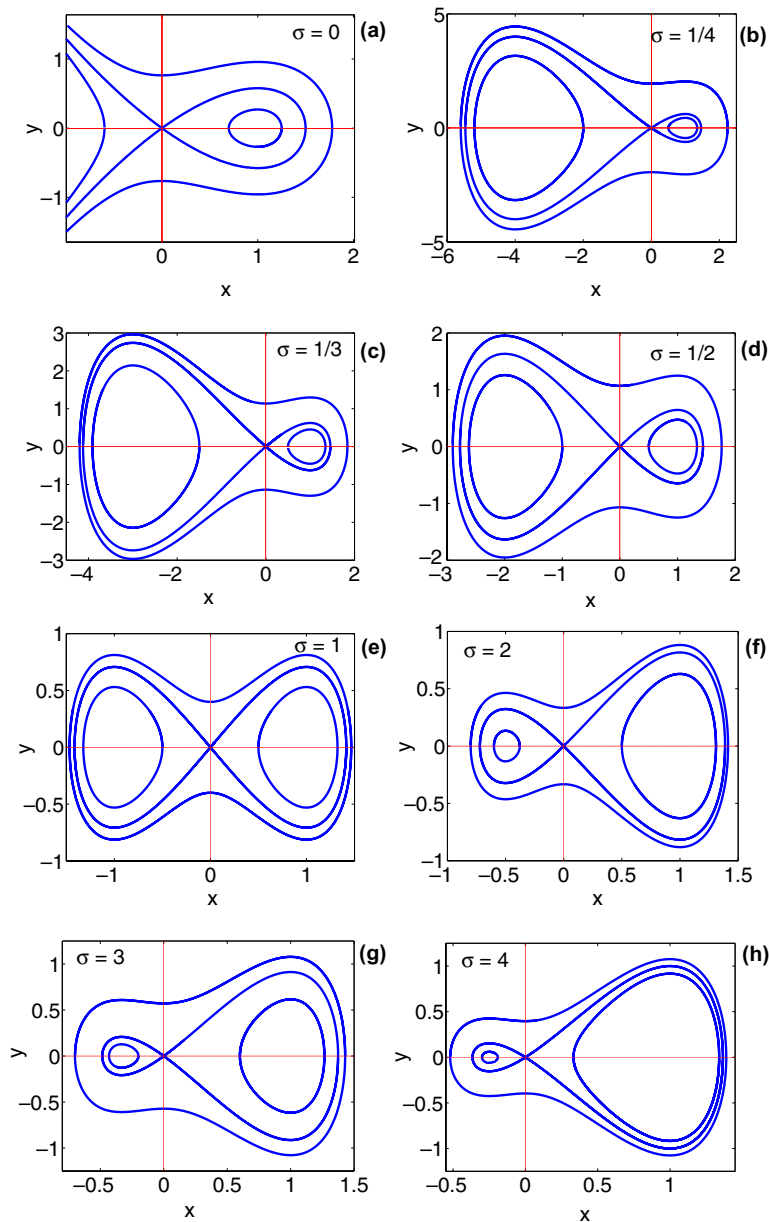


Fig. 2. Phase space portraits with respect to various values of parameter  $\sigma$ .

nously decreasing function, and especially tends to infinity when  $\sigma \rightarrow 0^+$  and tends to zero when  $\sigma \rightarrow +\infty$ ; the dotted line denotes the right-hand areas of the potential wells, which is different with our observation in Fig. 2. The areas of the right-hand potential wells will decrease slowly with the increase of  $\sigma$ , and tends gradually to a relative fixed value around 0.4. When  $\sigma = 1$ , the left-hand and the right-hand areas of the potential wells are the same.

It demonstrates that the right-hand side areas of potential wells of the unperturbed system vary only in a very small range around 0.4 no matter what values of  $\sigma$  are taken. While corresponding to the areas of the left-hand potential wells, when the symmetric parameter value  $\sigma$  varies, there exists a huge difference, and especially at both ends when  $\sigma$  tends to zero or infinity. Thus, due to the variation of  $\sigma$ , the phase space portraits of the unperturbed system will lead to the severe symmetry breaking phenomena, and especially in the left-hand size of the potential well. Much attention should be paid on the left-hand case of the Helmholtz–Duffing oscillator when  $\sigma \neq 1$ .

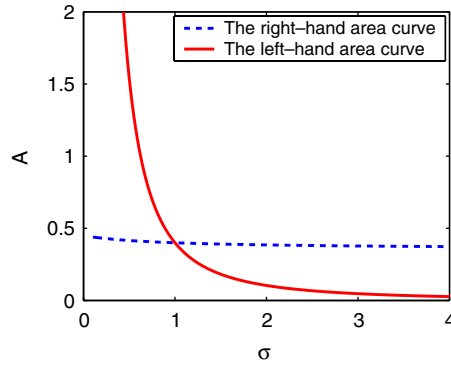


Fig. 3. Area curves of homoclinic orbits of the unperturbed system with respect to various values of parameter  $\sigma$ .

### 3. Local bifurcation analysis

In this section, in order to investigate the local bifurcation of the system Eq. (5) as the symmetric parameter  $\sigma$  varies at two different centers of the unperturbed system, we consider the primary harmonic solutions of the Helmholtz–Duffing oscillator when  $\sigma \neq 1$  using the second-order averaging method [20]. The main idea of this method is to change the non-autonomous dynamical system Eq. (5) into an autonomous dynamical system, then we may obtain the fixed points of the autonomous dynamical system (therefore we obtain the harmonic solutions of the original system Eq. (5)).

We choose first one center  $(x_0, 0)$  of the unperturbed system, then the frequency of the periodic orbit near the center is approximately by

$$\omega_0 = \sqrt{f'(x_0)}, \tag{15}$$

where  $f(x_0) = \sigma x_0^3 + (1 - \sigma)x_0^2 - x_0$ . If the ratio of  $\omega$  and  $\omega_0$  is a rational number, then the resonance behavior may occur. Here, we consider only the case of the primary resonance  $\omega \sim \omega_0$ .

Assume that

$$\epsilon\Omega = \omega^2 - \omega_0^2 \tag{16}$$

and

$$a_1 = f'(x_0), \quad a_2 = \frac{1}{2!}f''(x_0), \quad a_3 = \frac{1}{3!}f'''(x_0). \tag{17}$$

Then under the transformation

$$x = x_0 + \sqrt{\epsilon}z. \tag{18}$$

Eq. (5) can be rewritten in the following form:

$$\ddot{z} + \omega_0^2 z = -\sqrt{\epsilon}a_2 z^2 + \epsilon[\gamma \cos \omega t - a_3 z^3 - \delta \dot{z}] + \text{h.o.t}, \tag{19}$$

where h.o.t stands for the higher-order terms.

Using the van der Pol transformation

$$\begin{pmatrix} u \\ v \end{pmatrix} = \begin{pmatrix} \cos \omega t & -\frac{1}{\omega} \sin \omega t \\ -\sin \omega t & -\frac{1}{\omega} \cos \omega t \end{pmatrix} \begin{pmatrix} z \\ \dot{z} \end{pmatrix}, \tag{20}$$

and carrying out averaging up to second-order for Eq. (19), we obtain the following averaging equation:

$$\begin{cases} \dot{u} = \frac{\epsilon}{2\omega_0} [-\delta\omega_0 u + \Omega v - \beta_0(u^2 + v^2)v], \\ \dot{v} = \frac{\epsilon}{2\omega_0} [-\Omega u - \delta\omega_0 v + \beta_0(u^2 + v^2)u - \gamma], \end{cases} \tag{21}$$

where

$$\beta_0 = \frac{9a_1 a_3 - 10a_2^2}{12a_1}. \tag{22}$$

Via the polar coordinate transformation  $u = r \cos \theta$  and  $v = r \sin \theta$ , then Eq. (21) becomes

$$\begin{cases} \dot{r} = \frac{\epsilon}{2\omega_0} [-\delta\omega_0 r - \gamma \sin \theta], \\ r\dot{\theta} = \frac{\epsilon}{2\omega_0} [-\Omega r + \beta_0 r^3 - \gamma \cos \theta]. \end{cases} \quad (23)$$

The fixed points of Eq. (20) satisfy the following equation:

$$G(m) = \beta_0^2 m^3 - 2\Omega\beta_0 m^2 + (\Omega^2 + (\delta\omega_0)^2)m - \gamma^2 = 0, \quad (24)$$

where  $m = r^2$ . And the stabilities of the fixed points of Eq. (21) can be determined by the sign of the two roots of the equation:

$$m^2 + 2\delta\omega_0 m + H(m) = 0, \quad (25)$$

where  $H(m) = G'(m)$ .

In order to find the bifurcation values of the fixed points of Eq. (20) we write Eq. (24) as

$$F(n) = n^3 + pn + q = 0, \quad (26)$$

where

$$n = m + \frac{2\Omega}{3\beta_0}, \quad p = \frac{3\delta^2\omega_0^2 - \Omega^2}{3\beta_0^3}, \quad q = \frac{2\Omega^3 + 18\delta^2\omega_0^2\Omega - 27\beta_0\gamma^3}{27\beta_0^3}. \quad (27)$$

At the bifurcation points, Eq. (26) must have multiple roots, that is,

$$F(n) = 0, \quad \frac{\partial F}{\partial n} = 3n^2 + p = 0. \quad (28)$$

If we eliminate  $n$  from Eq. (26), then there is the following equation for a cusp results:

$$\Delta = 4p^3 + 27q^2 = 27\beta_0^2\gamma^4 - 4\beta_0\Omega(\Omega^2 + 9\delta^2\omega_0^2)\gamma^2 + 4\delta^2\omega_0^2(\Omega^2 + \delta^2\omega_0^2) = 0. \quad (29)$$

In view of the asymmetry of Helmholtz–Duffing oscillator when  $\sigma \neq 1$ , there exist two different centers, so we discuss the left-hand side center  $(-1/\sigma, 0)$  and the right-hand side center  $(1, 0)$ , respectively.

*Case I.* At the right-hand center  $(1, 0)$ .

We at first give some parameters related to the right-hand center  $(1, 0)$  as follows:

$$\begin{aligned} a_1 &= 1 + \sigma, & a_2 &= 2\sigma + 1, & a_3 &= \sigma, \\ \beta_0 &= -\frac{31\sigma^2 + 31\sigma + 10}{12(\sigma + 1)} < 0 \quad (\sigma > 0), & \omega_0 &= \sqrt{a_1}. \end{aligned} \quad (30)$$

Obviously, these parameters are dependent on  $\sigma$ .

If we fix  $\delta = 0.1$ ,  $\epsilon = 0.1$ , and change  $\Omega$  into  $(\omega^2 - \omega_0^2)/\epsilon$ , then corresponding to various values of parameter  $\sigma$ , we have a supercritical saddle-node bifurcation curve  $\gamma_1$  and a subcritical saddle-node bifurcation curve  $\gamma_2$  of the fixed points of Eq. (20) as follows:

$$\gamma_{1,2} = \sqrt{\frac{2\Omega(\Omega^2 + 9\delta^2\omega_0^2) \mp 2(\Omega^2 - 3\delta^2\omega_0^2)\sqrt{\Omega^2 - 3\delta^2\omega_0^2}}{27\beta_0}} \begin{cases} 0 \leq \omega \leq 1.2161, & \sigma = \frac{1}{2}, \\ 0 \leq \omega \leq 1.1460, & \sigma = \frac{1}{3}, \\ 0 \leq \omega \leq 1.1093, & \sigma = \frac{1}{4}, \\ 0 \leq \omega \leq 1.0867, & \sigma = \frac{1}{5}. \end{cases} \quad (31)$$

From the averaging theorem [20], a stable resonant harmonic appears near the curve  $\gamma_1$  and a stable non-resonant harmonic disappears near the curve  $\gamma_2$ .

Seen from Fig. 4(a), there exist different saddle-node bifurcation curves corresponding to different values of parameters  $\sigma$ , and the range of frequency  $\omega$  will decrease gradually with the decrease of  $\sigma$ .

*Case II.* At the left-hand center  $(-1/\sigma, 0)$ .

Due to the asymmetry between the left-hand center and the right-hand one, we give other parameters related to the left-hand side center  $(-1/\sigma, 0)$  as follows:

$$\begin{aligned} a_1 &= 1 + \frac{1}{\sigma}, & a_2 &= -(2 + \sigma), & a_3 &= \sigma, \\ \beta_0 &= -\frac{\sigma(10\sigma^2 + 31\sigma + 31)}{12(\sigma + 1)} < 0 \quad (\sigma > 0), & \omega_0 &= \sqrt{a_1}. \end{aligned} \quad (32)$$

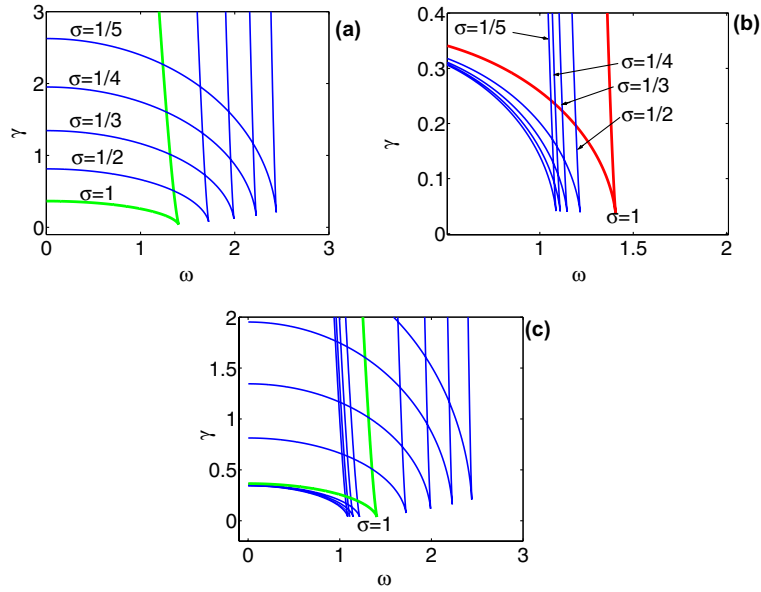


Fig. 4. Supercritical and subcritical saddle-node bifurcation curves with respect to various values of parameter  $\sigma$ , where (a) at the left-hand center; (b) at the right-hand center; (c) at the left-hand and right-hand centers.

Also, we have the following two saddle-node bifurcation curves of the fixed points of Eq. (20) shown in Fig. 4(b):

$$\gamma_{3,4} = \sqrt{\frac{2\Omega(\Omega^2 + 9\delta^2\omega_0^2) \mp 2(\Omega^2 - 3\delta^2\omega_0^2)\sqrt{\Omega^2 - 3\delta^2\omega_0^2}}{27\beta_0}} \begin{cases} 0 \leq \omega \leq 1.7234, & \sigma = \frac{1}{2}, \\ 0 \leq \omega \leq 1.9913, & \sigma = \frac{1}{3}, \\ 0 \leq \omega \leq 2.2274, & \sigma = \frac{1}{4}, \\ 0 \leq \omega \leq 2.4408, & \sigma = \frac{1}{5}, \end{cases} \quad (33)$$

where  $\gamma_3$  corresponds to a supercritical saddle-node bifurcation curve, and  $\gamma_4$  is a subcritical saddle-node bifurcation curve of the fixed points of Eq. (20). Different with that case in right-hand center, there exist different saddle-node bifurcation curves corresponding to various parameters  $\sigma$ . The range of the frequency  $\omega$  will increase gradually with the decrease of  $\sigma$ .

Fig. 4(c) shows that the parameter plane  $(\omega, \gamma)$  can be divided into different parts resulting from different saddle-node bifurcation curves corresponding to the left-hand and the right-hand centers, and in each part there exist different fixed points of Eq. (20). Therefore, from the averaging theorem [20], these fixed points of Eq. (20) correspond to different harmonics of Eq. (5).

The advantage using the second-order averaging method is to obtain the local bifurcations at two different centers of the system, separately. These results show that the local saddle-node bifurcations are asymmetric with respect to different parameter values  $\sigma$  at the left-hand and the right-hand centers. The regions resulting from the left-hand saddle-node bifurcation curves will produce the transition toward the right when the parameter  $\sigma$  ( $\sigma < 1$ ) decreases; when  $\sigma = 1$ , the right-hand saddle-node bifurcation curve and the right-hand one are the same. The region resulting from the right-hand saddle-node bifurcation curves will be transformed to the left-hand when the parameter  $\sigma$  ( $\sigma < 1$ ) decreases.

When  $\sigma > 1$ , there exist still two different centers at  $(-1/\sigma, 0)$  and  $(1, 0)$ , and the results are similar with that when  $0 < \sigma < 1$ , so we omit the related discussion.

#### 4. Melnikov analysis

To study the global bifurcation, we are mainly concerned with the Melnikov analysis [21,22]. First, a new variable is introduced as  $\phi = \omega t$ , and  $\dot{\phi} = d\phi/dt = \omega$ , so we can rewrite Eq. (5) in an extended form as

$$\begin{aligned} \dot{x} &= y, \\ \dot{y} &= x - (1 - \sigma)x^2 - \sigma x^3 - \delta y + \gamma \cos(\phi), \\ \dot{\phi} &= \omega. \end{aligned} \quad (34)$$

Poincaré section  $\Sigma$  may be taken as

$$\Sigma = \{(x, y, \phi) \in \mathbf{R}^2 \times S^1 | \phi = 0\}, \tag{35}$$

in which  $S^1$  is a unit circle with longitude  $2\pi$ , and the phase space of Eq. (34) is  $\mathbf{R}^2 \times S^1$ , then the Poincaré map can be defined as

$$P : (x(0), y(0)) \rightarrow (x(T), y(T)), \tag{36}$$

where  $(x, y, \phi) = (x(t), y(t), \omega t)$  is a solution of Eq. (34), and  $T = 2\pi/\omega$ .

The Melnikov function is defined as follows:

$$\begin{aligned} M^{r,l}(t_0) &= \int_{-\infty}^{\infty} y_0^{r,l}(t) \{-\delta y_0^{r,l}(t) + \gamma \cos \omega(t + t_0)\} dt \\ &= -\delta \int_{-\infty}^{\infty} [y_0^{r,l}(t)]^2 dt - \left[ \gamma \sin(\omega t_0) \int_{-\infty}^{\infty} y_0^{r,l}(t) \sin(\omega t) dt \right] \\ &= -\delta B^{r,l} - \gamma \sin(\omega t_0) I^{r,l}(\omega), \end{aligned} \tag{37}$$

where

$$\begin{aligned} B^{r,l} &= \int_{-\infty}^{\infty} [y_0^{r,l}(t)]^2 dt, \\ I^{r,l}(\omega) &= \int_{-\infty}^{\infty} y_0^{r,l}(t) \sin(\omega t) dt. \end{aligned} \tag{38}$$

Suppose that the Melnikov function has a simple zero point, then the homoclinic bifurcations can be deduced from Eq. (37) as follows:

$$\gamma_{\text{crh}}^{r,l}(\omega) = \frac{\delta B^{r,l}}{I^{r,l}(\omega)}, \tag{39}$$

where the subscripts ‘‘crh’’ stands for the critical homoclinic bifurcation value.

In general,  $\gamma_{\text{crh}}^r(\omega) \neq \gamma_{\text{crh}}^l(\omega)$  when the asymmetric parameter  $\sigma \neq 1$ .

According to Melnikov’s theory [21,22], if there exists a simple zero point  $t_0$  of the Melnikov function  $M^{r,l}(t_0)$ , then there exist the homoclinic intersections on the left and right parts of the phase space if and only if  $\gamma^{r,l}(\omega) > \gamma_{\text{crh}}^{r,l}(\omega)$  is satisfied, where  $\gamma^{r,l}(\omega)$  represents an amplitude coefficient that is larger than the right-hand and the left-hand critical homoclinic bifurcation values in the frequency–amplitude parameter plane  $(\omega, \gamma)$ .

Thus, two homoclinic bifurcation curves  $\gamma_{\text{crh}}^{r,l}(\omega)$  can be obtained in the frequency–amplitude parameter plane  $(\omega, \gamma)$ , respectively. The frequency–amplitude parameter plane  $(\omega, \gamma)$  can be divided into three parts: one is the zone where both the left-hand and the right-hand homoclinic intersections do not occur (below the two critical curves); one is the zone where only the left-hand or the right-hand homoclinic intersection occurs (one is below a critical curve and the other is above another critical curve); one is the zone where both the left-hand and the right-hand homoclinic intersections occur (above the two critical curves), and according to the Smale–Birkhoff homoclinic theory, Eq. (34) exhibits chaotic motions.

We fix the damping coefficient  $\delta = 0.1$  and let the frequency  $\omega$  varying in the range  $(0, 4)$ , and then take different values of parameter  $\sigma$ . The parameter plane  $(\omega, \gamma)$  can be divided into different parts shown in Fig. 5. Due to  $\gamma_{\text{crh}}^r(\omega) \neq \gamma_{\text{crh}}^l(\omega)$ , there exist two different homoclinic bifurcation curves with respect to each  $\sigma$  ( $\sigma \neq 1$ ).

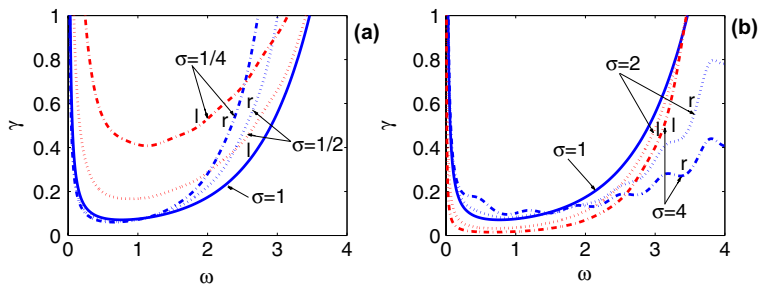


Fig. 5. Homoclinic bifurcations with respect to various values of parameter  $\sigma$ , where (a)  $\sigma < 1$ ; (b)  $\sigma > 1$ .

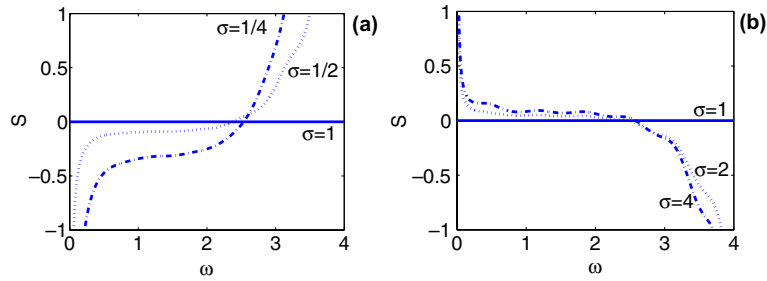


Fig. 6. Symmetric functions with respect to various values of parameter  $\sigma$ , where (a)  $\sigma < 1$ ; (b)  $\sigma > 1$ .

In Fig. 5(a), all homoclinic bifurcation curves are obtained from Eq. (39) with respect to some representative parameters  $\sigma < 1$ , while Fig. 5(b) corresponds to other homoclinic bifurcation curves when  $\sigma > 1$ . And for the sake of comparison, the solid curve denotes the homoclinic bifurcation curve when  $\sigma = 1$ .

From Fig. 5, it is shown that when the parameter  $\sigma \neq 1$ , the left-hand and the right-hand homoclinic bifurcations are asymmetric. In particular, there always exist a critical frequency  $\omega_c$ , at which the left-hand homoclinic bifurcation value is equal to the right-hand homoclinic bifurcation value; in addition to the critical frequency  $\omega_c$ , the left-hand homoclinic bifurcation value is different to the right-hand one. When  $\sigma < 1$  and  $\omega < \omega_c$ ,  $\gamma_{\text{crh}}^l > \gamma_{\text{crh}}^r$ ; while if  $\omega > \omega_c$ , then  $\gamma_{\text{crh}}^l < \gamma_{\text{crh}}^r$ . The results are just reversed when  $\sigma > 1$ .

To further study the difference between the left-hand and right-hand homoclinic bifurcations, a *symmetric function* is defined by the following equation:

$$s(\omega) = \gamma_{\text{crh}}^r(\omega) - \gamma_{\text{crh}}^l(\omega). \quad (40)$$

Fig. 6 presents the symmetric function with respect to different values of parameter  $\sigma$ , in which one can clearly see that when the parameter  $\sigma < 1$ , the symmetric function is a monotonously increasing function, while when the parameter  $\sigma > 1$ , the symmetric function becomes a monotonously decreasing function. There exist always a critical frequency  $\omega_c$ , by which each symmetric function has a zero point, which means that the left-hand homoclinic bifurcation value is equal to the right-hand homoclinic bifurcation value at the critical frequency  $\omega_c$ . In addition to the critical frequency  $\omega_c$ , the left-hand homoclinic bifurcation value is different to the right-hand one.

Seen from Fig. 6(a), note that when  $\sigma < 1$  and  $\omega < \omega_c$ , the homoclinic bifurcation value will increase with the increase of  $\sigma$ ; while when  $\omega > \omega_c$ , the homoclinic bifurcation value will decrease with the increase of  $\sigma$ . These results are just reversed when  $\sigma > 1$ . Thus, the symmetry parameter  $\sigma$  can affect the occurrence of homoclinic intersections as  $\sigma$  varies. In general, the occurrence is always non-synchronization between the left-hand homoclinic manifolds and the right-hand ones. Due to the asymmetry, much attention should be placed on the large homoclinic bifurcation value. Making use of these results, the local transversal intersections of the left-hand homoclinic manifolds or the right-hand ones can be suppressed or induced by adjusting the symmetric parameter  $\sigma$  in advance. In view of these results above, two scenarios concerning the local and global stabilities of the system can be considered in the following numerical simulations.

## 5. Numerical simulations

In this section, we will plot the skeletons and the basins of attraction of the Helmholtz–Duffing oscillator corresponding to two cases, and see what happen under the effect of the symmetric parameter  $\sigma$ .

### 5.1. Local stability

At first, we consider the first case when  $\sigma < 1$  and  $\omega = 1$ .

#### 5.1.1. The skeletons of the system

When  $\sigma = 1/2$ , from Eq. (39), the left-hand and the right-hand homoclinic bifurcation values are  $\gamma_{\text{crh}}^l = 0.1679$ , and  $\gamma_{\text{crh}}^r = 0.0723$ , respectively. The left-hand homoclinic bifurcation is approximately 2.3 times of the right-hand one.

When  $\gamma_{\text{crh}}^l = 0.1679$ , this is a larger homoclinic bifurcation than the right-hand homoclinic bifurcation value. So seen from Fig. 7(a), when the left-hand stable and unstable manifolds are tangent, the right-hand stable and unstable manifolds have produced the intensively transversal intersections.

On the other hand, if we take the small right-hand critical homoclinic bifurcation value  $\gamma_{\text{crh}}^r = 0.0723$ , then we see that from Fig. 7(b), although the right-hand stable manifold and unstable manifold are in the tangent state, the left-hand stable and unstable manifolds are in the separation state. Therefore, the effect resulting from the small homoclinic bifurcation for the global dynamics of the system is local, and the system is still in a kind of stability state.

If we take  $\gamma = 0.4 > \gamma_{\text{crh}}^l$ , then seen from Fig. 8(a), the left-hand homoclinic manifolds have produced the transversal intersections, and the intensity of transversal intersections of the left-hand homoclinic manifolds is quite larger than the right-hand one. Under this situation, the global stability of the system could be destroyed. If we take  $\gamma = 0.1$  between  $\gamma_{\text{crh}}^l$  and  $\gamma_{\text{crh}}^r$ , then seen from Fig. 8(b), although the right-hand homoclinic manifolds have produced the transversal intersections, the left-hand homoclinic manifolds are still in the separation state. That is to say, if we take the amplitude coefficient  $\gamma$  between the small right-hand critical homoclinic bifurcation and the large left-hand one, then the global stability of the system does not receive much more influence.

If we decrease the parameter  $\sigma$  to  $1/4$ , then the left-hand and the right-hand homoclinic bifurcations are  $\gamma_{\text{crh}}^l = 0.4132$ , and  $\gamma_{\text{crh}}^r = 0.072$ , respectively. At this situation, the left-hand homoclinic bifurcation is approximately 5.74 times of the right-hand one. Seen from Fig. 9, the similar case occurs as that shown in Fig. 7, but there is a little

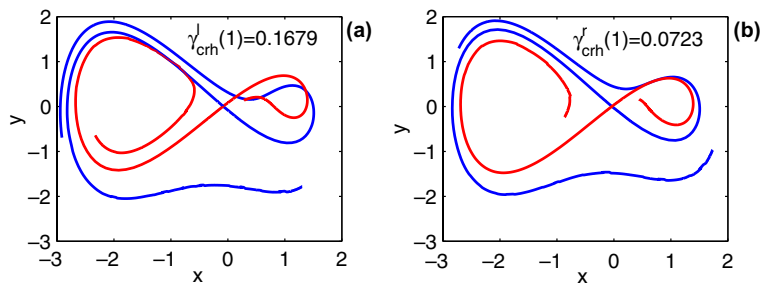


Fig. 7. Stable manifolds and unstable manifolds with respect to parameters  $\sigma = 1/2$  and  $\omega = 1$ , where (a)  $\gamma_{\text{crh}}^l = 0.1679$  and (b)  $\gamma_{\text{crh}}^r = 0.0723$ .

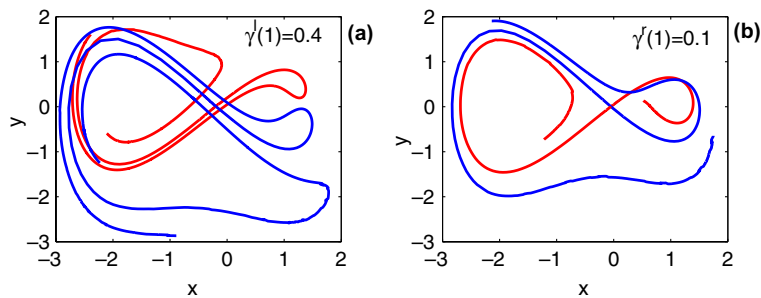


Fig. 8. Stable manifolds and unstable manifolds with respect to parameters  $\sigma = 1/2$  and  $\omega = 1$ , where (a)  $\gamma^l = 0.4$  and (b)  $\gamma^r = 0.1$ .

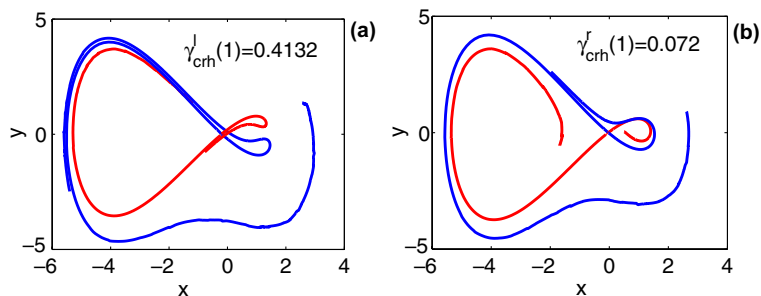


Fig. 9. Stable manifolds and unstable manifolds with respect to parameters  $\sigma = 1/4$  and  $\omega = 1$ , where (a)  $\gamma_{\text{crh}}^l = 0.4132$  and (b)  $\gamma_{\text{crh}}^r = 0.072$ .

difference. The size of the left-hand homoclinic tangle shown in Fig. 7 is less than the size of the left-hand one shown in Fig. 9 when  $\sigma = 1/4$ . So with the increase of parameter  $\sigma$ , the effect for the left-hand homoclinic tangle will be weaken.

If we change the above case from  $\sigma < 1$  into  $\sigma > 1$ , then the similar situation occurs as those when  $\sigma < 1$ . The detailed variations can be seen from Figs. 10 and 11.

### 5.1.2. The basins of attraction

In the above subsection, we plot the skeleton of the Helmholtz–Duffing oscillator when the parameter  $\sigma$  varies, and we obtain various patterns between the stable and unstable manifolds of the Poincaré map. In this subsection, the basins of attraction will be used to further observe what happen from the global point of view.

Two cases will be considered as follows.

*Case I.* When  $\sigma = 1/4$ , we take the corresponding left-hand homoclinic bifurcation value as  $\gamma_{\text{crh}}^{\text{l}} = 0.4132$ . Seen from Fig. 12(a), there exist three different attractors, in which one is attracted to the right-hand potential well; one is attracted to the left-hand potential well; and the third one is located in the middle-upper part of the basin of attraction. Due to  $\gamma_{\text{crh}}^{\text{l}} > \gamma_{\text{crh}}^{\text{r}} = 0.072$ , the boundaries of the right-hand and the middle-upper attractors cause the weak fractal-like structure, while the right-hand homoclinic tangle of the Poincaré map has eroded the right-hand potential well and the middle-upper part of the basin of attraction. Different with the right-hand case, the left-hand attractor has no any erosion phenomenon occurring and its boundary is basically smooth.

If we increase the amplitude coefficient to  $\gamma = 2$ , which is far larger than the above both-side critical homoclinic bifurcation values, then seen from Fig. 12(b), the severe erosion phenomenon occurs in the right-hand potential well. At the same time, the left-hand potential well has been penetrated partly by the right-hand homoclinic tangles.

If we take the relatively small right-hand homoclinic bifurcation as  $\gamma_{\text{crh}}^{\text{r}} = 0.072$ , then we see three attractors shown in Fig. 12(c). Their boundaries of the three attractors are smooth. And there exist a huge difference in sizes between the left-hand and right-hand attractors.

*Case II.* When  $\sigma = 4$ , we take the left-hand homoclinic bifurcation as  $\gamma_{\text{crh}}^{\text{l}} = 0.018$  and the right-hand homoclinic bifurcation as  $\gamma_{\text{crh}}^{\text{r}} = 0.1012$ . Seen from Fig. 13, the basic patterns are the similar as those shown in Fig. 12.

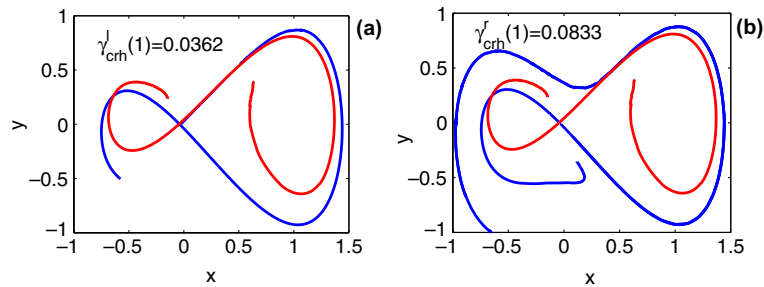


Fig. 10. Stable manifolds and unstable manifolds with respect to parameters  $\sigma = 2$  and  $\omega = 1$ , where (a)  $\gamma_{\text{crh}}^{\text{l}} = 0.0362$  and (b)  $\gamma_{\text{crh}}^{\text{r}} = 0.0833$ .

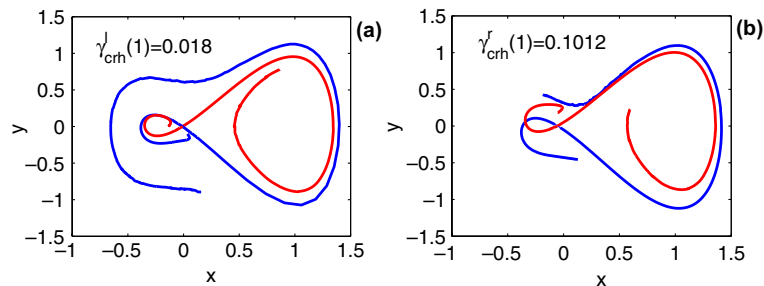


Fig. 11. Stable manifolds and unstable manifolds with respect to parameters  $\sigma = 4$  and  $\omega = 1$ , where (a)  $\gamma_{\text{crh}}^{\text{l}} = 0.018$  and (b)  $\gamma_{\text{crh}}^{\text{r}} = 0.1012$ .

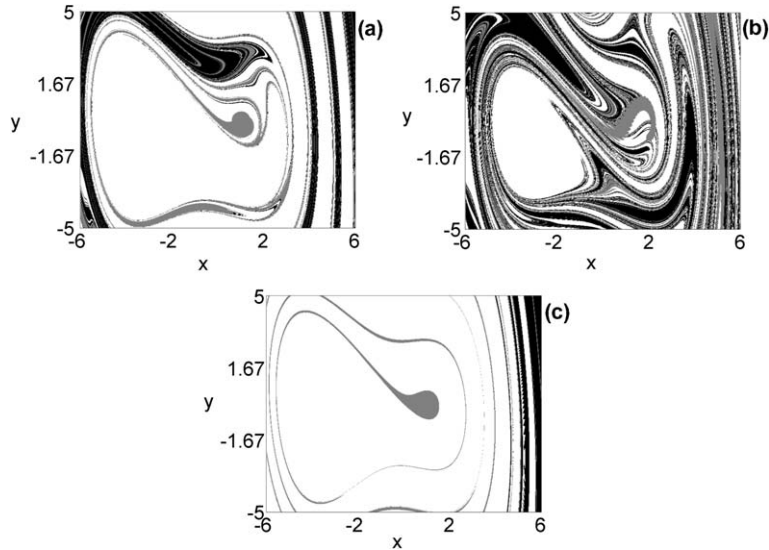


Fig. 12. The basins of attraction with respect to parameter  $\sigma = 1/4$  and  $\omega = 1$ , where (a)  $\gamma_{\text{crh}}^l = 0.4135$ ; (b)  $\gamma = 2$ ; (c)  $\gamma_{\text{crh}}^r = 0.072$ .

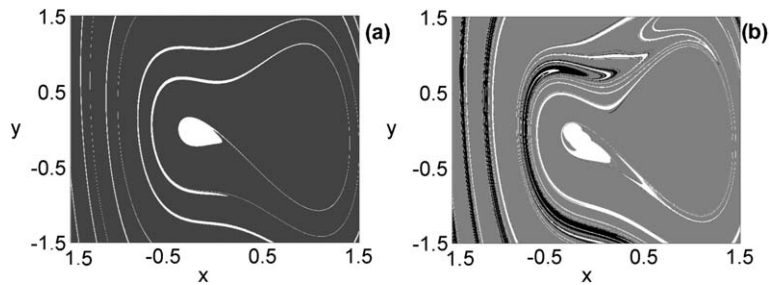


Fig. 13. The basins of attraction with respect to parameters  $\sigma = 4$  and  $\omega = 1$ , where (a)  $\gamma_{\text{crh}}^l = 0.018$  and (b)  $\gamma_{\text{crh}}^r = 0.1012$ .

## 5.2. Global stability

### 5.2.1. The skeletons of the system

For simplicity, we can only consider one case when  $\sigma = 1/2$ . From Melnikov analysis, there exists a critical frequency  $\omega_c = 2.378$ , by which the left-hand and the right-hand homoclinic bifurcations attain the same value,  $\gamma_{\text{crh}}^l = \gamma_{\text{crh}}^r = 0.3835$ . The skeleton shown in Fig. 14(a) demonstrates that the left-hand and the right-hand stable and unstable manifolds of Poincaré map are in the tangent state, simultaneously.

If we further increase the homoclinic bifurcation value to  $\gamma = 0.5$ , then the left-hand and the right-hand stable and unstable manifolds of Poincaré map will lead to severely transversal intersections. Fig. 14(b) identifies this fact.

### 5.2.2. The basins of attraction

Corresponding to the skeleton shown in Fig. 14, the basins of attraction are given in Fig. 15. As we first see from Fig. 15(a), the critical global homoclinic bifurcation value is  $\gamma_{\text{crh}} = 0.3835$  at the critical frequency  $\omega_c = 2.378$ . The boundaries of the left-hand and the right-hand attractors cause a little fractal-like structure. When the parameter  $\gamma$  is increased to 0.5, seen from Fig. 15(b), the fractal boundaries of the left-hand and right-hand attractors are much more obvious than that presented in Fig. 15(a). The right-hand internal erosion of the potential well is also much more obvious than that shown in Fig. 15(a). It demonstrates that the original stable and bounded oscillations have escaped from the right-hand potential well. At the same time, the left-hand internal erosion phenomenon of the potential well also occurs.

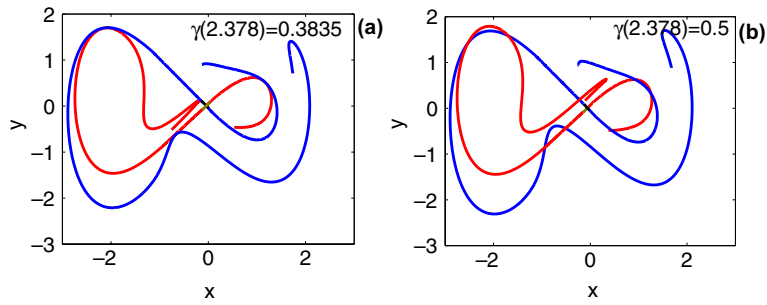


Fig. 14. The skeleton of stable and unstable manifolds with respect to parameters  $\sigma = 1/2$  and  $\omega_c = 2.378$ , where (a)  $\gamma = 0.3835$  and (b)  $\gamma = 0.5$ .

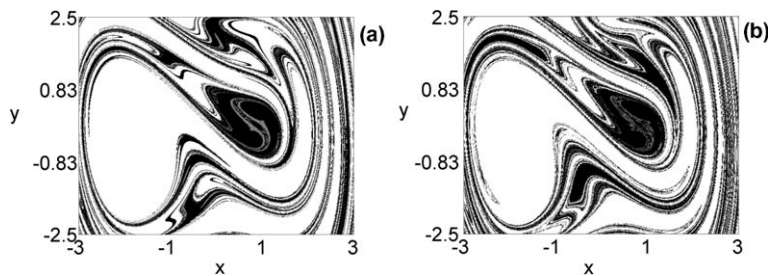


Fig. 15. The basins of attraction with respect to parameters  $\sigma = 1/2$  and  $\omega_c = 2.378$ , where (a)  $\gamma = 0.3835$  and (b)  $\gamma = 0.5$ .

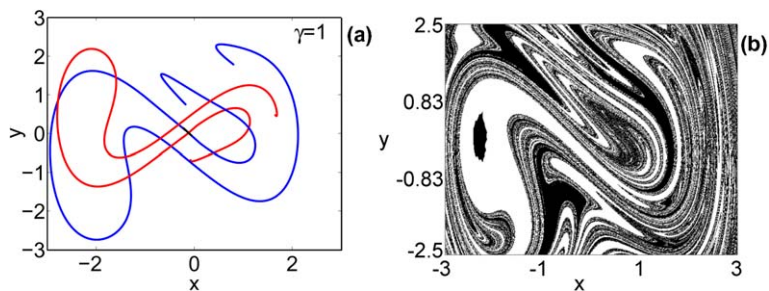


Fig. 16. (a) The skeleton of stable and unstable manifolds, and (b) the basin of attraction with respect to parameters  $\sigma = 1/2$ ,  $\omega_c = 2.378$ , and  $\gamma = 1$ .

If the parameter  $\gamma$  further increase. The detailed patterns can be seen from Fig. 16. Note that the amplitude coefficient is only half of that in Fig. 12(b), but the intensity of the global instability shown in Fig. 16(b) is larger than that in Fig. 12(b). Thus, if a relatively large amplitude coefficient is taken as a control parameter at the critical frequency  $\omega_c$ , then the global stability of this system will be destroyed at a lowest cost. Otherwise, under the case of the asymmetric homoclinic bifurcation when  $\omega \neq \omega_c$ , the same effects can be realized but it must be paid at a largest cost.

## 6. Conclusions and discussion

We have investigated various symmetry breaking phenomena in a general Helmholtz–Duffing oscillator when a symmetric parameter varies. These symmetry breaking phenomena are strongly dependent on the symmetry parameter. Due to the variation of the symmetry parameter, the phase space patterns of the unperturbed system, the local saddle-node bifurcations, and the global homoclinic bifurcations can be represented as different function relations of the symmetry parameter.

All results can be traced back to the basic fact that the left-hand side areas of the homoclinic orbits of the unperturbed Helmholtz–Duffing oscillator can produce the substantial changes from zero to infinity when  $\sigma$  varies, while the right-hand side areas of homoclinic orbits can remain in the relatively stable state.

Due to this basic fact, when the symmetric parameter varies, the symmetry breaking phenomena are always existing besides the case  $\sigma = 1$ , including the variation of the patterns of the phase space portraits of the unperturbed system, the transition of the local saddle-node bifurcations in the frequency–amplitude plane, as well as the non-synchronistic transversal intersections induced by different homoclinic bifurcations between the left-hand homoclinic orbit and the right-hand one.

One of our main findings demonstrates that much attention should be paid on the case that both sides can attain the same homoclinic bifurcation value at some critical frequency. Corresponding to the same homoclinic bifurcation value, the stable and unstable manifolds of the Poincaré map will cause the synchronic tangency in both sides of potential wells. If we take the amplitude coefficient as a control parameter, which is quite larger than the same critical homoclinic bifurcation, then both sides will lead to the severely synchronic transversal intersections between the stable and unstable manifolds of the Poincaré map. The numerical simulations identify that if this kind of global homoclinic tangle occurs, then the erosions occurring in both sides of the potential wells will lead to the fractal-like boundaries of the basins of attraction. And the original stable and bounded oscillations will escape from both sides of potential wells. Finally, the global stability of the system will be destroyed.

In addition, the effects for the system's stability resulting from asymmetric homoclinic bifurcations are different. The small homoclinic bifurcation does not affect the global stability of this system even though the one-side homoclinic tangle occurs. Thus the effect resulting from the small homoclinic bifurcation for the system's stability is local and negligible. The large homoclinic bifurcation can lead to the instability of the global system, but this is accomplished at a quite larger cost. Usually, the amplitude coefficient must be taken as large as possible. Different with the case, the same critical homoclinic bifurcation value is an optimal value. If the amplitude coefficient is larger than the same critical homoclinic bifurcation value, and can be used to be a control parameter at the critical frequency, then the system's global stability will be destroyed at a lowest cost.

## Acknowledgments

This work is supported by the Program of Mobility of Foreign Researchers by the State Secretary of Universities and Research of the Spanish Ministry of Education and Science under the project number SB2004-002 (H. Cao), and by the Spanish Ministry of Science and Technology under project number BFM2003-03081. H. Cao acknowledges the warm hospitality received at Universidad Rey Juan Carlos where this work was carried out. We would like to thank Samuel Zambrano for his help improving the quality of the figures of this paper.

## References

- [1] Sofroniou A, Bishop SR. Breaking the symmetry of the parametrically excited pendulum. *Chaos, Solitons & Fractals* 2006;28:673–81.
- [2] Isohätälä J, Alekseev KN, Kurki LT, Pietiläinen P. Symmetry breaking in a driven and strongly damped pendulum. *Phys Rev E* 2005;71:066201–6.
- [3] Bishop SR, Sofroniou A, Shi P. Symmetry-breaking in the response of the parametrically excited pendulum. *Chaos, Solitons & Fractals* 2005;25:257–64.
- [4] Lai YC. Symmetry-breaking bifurcation with on-off intermittency in chaotic dynamical systems. *Phys Rev E* 1996;53:4267–70.
- [5] Yamgoué SB, Kofané TC. Chaotic responses of a deformable system under parametric and external excitations. *Chaos, Solitons & Fractals* 2003;17:155–67.
- [6] Abed EH, Varaiya PP. Nonlinear oscillations in power systems. *Int J Electron Power Energy Syst* 1984;6:37.
- [7] Abed EH, Wang HD, Alexander JC, Hamdan AMA, Lee HC. Dynamic bifurcations in a power system model exhibiting voltage collapse. *Int J Bifurcat Chaos* 1993;3:1170–80.
- [8] Ajarapu V, Lee B. Bifurcation theory and its application to nonlinear dynamical phenomena in an electrical power system. *Trans Power Syst* 1992;17(1):424–31.
- [9] Dobson I, Chiang HD. Towards a theory of voltage collapse in electric power systems. *Syst Control Lett* 1989;13:253–62.
- [10] Moon FC. *Chaotic and fractal dynamics: a introduction for applied scientists and engineers*. John Wiley & Sons Inc.; 1992.
- [11] Yagasaki K. Chaos in a pendulum with feedback control. *Nonlinear Dyn* 1994;6:125–42.
- [12] Litvak-Hinenzon A, Rom-Kedar V. Symmetry-breaking perturbations and strange attractors. *J Sound Vib* 1997;55:4964–78.
- [13] Lenci S, Rega G. Optimal control of nonregular dynamics in a Duffing oscillator. *Nonlinear Dynam* 2003;33:71–86.

- [14] Lenci S, Rega G. Global optimal control and system-dependent solutions in the hardening Helmholtz–Duffing oscillator. *Chaos, Solitons & Fractals* 2004;21:1031–46.
- [15] Almendral JA, Seoane J, Sanjuán MAF. Nonlinear dynamics of the Helmholtz oscillator. *Recent Res Devel Sound Vib* 2004;2:115–50.
- [16] Almendral JA, Sanjuán MAF. Integrability and symmetry for the Helmholtz oscillator with friction. *J Phys A: Math Gen* 2003;36:695.
- [17] Sanjuán MAF. The effect of nonlinear damping on the universal escape oscillator. *Int J Bifurcat Chaos* 1999;9:735–44.
- [18] Metter E. Dynamic buckling. In: Flügge W, editor. *Handbook of engineering mechanics*. NY: Wiley; 1992.
- [19] Bkdash M, Balachandran B, Nayfeh A. Melnikov analysis for a ship with a general roll-damping model. *Nonlinear Dyn* 1994;6:101–24.
- [20] Yagasaki K. Second-order averaging and Melnikov analysis for forced nonlinear oscillators. *Nonlinear Dyn* 1996;190:587–609.
- [21] Guckenheimer J, Holmes P. *Nonlinear oscillations, dynamical systems, and bifurcations of vector fields*. NY: Springer-Verlag; 1983.
- [22] Wiggins S. *Introduction to applied nonlinear dynamical systems and chaos*. NY: Springer-Verlag; 1990.